

Article

Fast and Selective Degradation of Biomass for Xylose, Glucose and Lignin under Mild Conditions

Shangzhong Zhang¹, Yi Duan^{1,2}, Changchang Teng¹, Hongdong Quan¹, Xiuguo Yang³, Hongyan Li³, Xiaohu Li³ and Lifeng Yan^{1,*} 

¹ Department of Chemical Physics, University of Science and Technology of China, Jinzai Road 96, Hefei 230026, China

² Key Laboratory of Anhui for Tobacco Chemistry, Hefei 230088, China

³ Inner Mongolia Key Laboratory of Polyol Chemical New Material Enterprise, Chifeng Ruiyang Chemical Co., Ltd., Pingzhuang, Chifeng 024076, China

* Correspondence: lfyang@ustc.edu.cn

Abstract: The conversion of lignocellulose into valuable chemicals has been recognized as the key technology in green chemistry. However, selective degradation of hemicellulose and cellulose with the production of lignin is still a challenge. Therefore, a two-step process has been developed to degrade corncob into xylose and glucose under mild conditions. At first, the corncob was treated with the lower concentration of zinc chloride aqueous solution (30–55 w%) at 95 °C with a short reaction time (8–12 min) and 30.4 w% (selectivity = 89%) of xylose obtained with a solid residue of the composite of cellulose and lignin. Next, the solid residue was treated with a high concentration of zinc chloride aqueous solution (65–85 w%) at 95 °C for about 10 min, and 29.4 w% (selectivity = 92%) of glucose can be obtained. Combining the two steps, the total yield of xylose is 97%, while glucose is 95%. In addition, high pure lignin can be obtained simultaneously, which was confirmed using HSQC studies. Furthermore, for the solid residue of the first-step reaction, a ternary deep eutectic solvent (DES) (choline chloride/oxalic acid/1,4-butanediol, ChCl/OA/BD) has been used to separate the cellulose and lignin efficiently, and high-quality cellulose (Re-C) and lignin (Re-L) were obtained. Furthermore, it provides a simple method to disassemble the lignocellulose for monosaccharides, lignin, and cellulose.

Keywords: lignocellulose; corncob; glucose; xylose; lignin



Citation: Zhang, S.; Duan, Y.; Teng, C.; Quan, H.; Yang, X.; Li, H.; Li, X.; Yan, L. Fast and Selective Degradation of Biomass for Xylose, Glucose and Lignin under Mild Conditions. *Molecules* **2023**, *28*, 3306. <https://doi.org/10.3390/molecules28083306>

Academic Editors: Ola Sundman and Carlos Martin

Received: 27 February 2023

Revised: 6 April 2023

Accepted: 6 April 2023

Published: 7 April 2023



Copyright: © 2023 by the authors. Licensee MDPI, Basel, Switzerland. This article is an open access article distributed under the terms and conditions of the Creative Commons Attribution (CC BY) license (<https://creativecommons.org/licenses/by/4.0/>).

1. Introduction

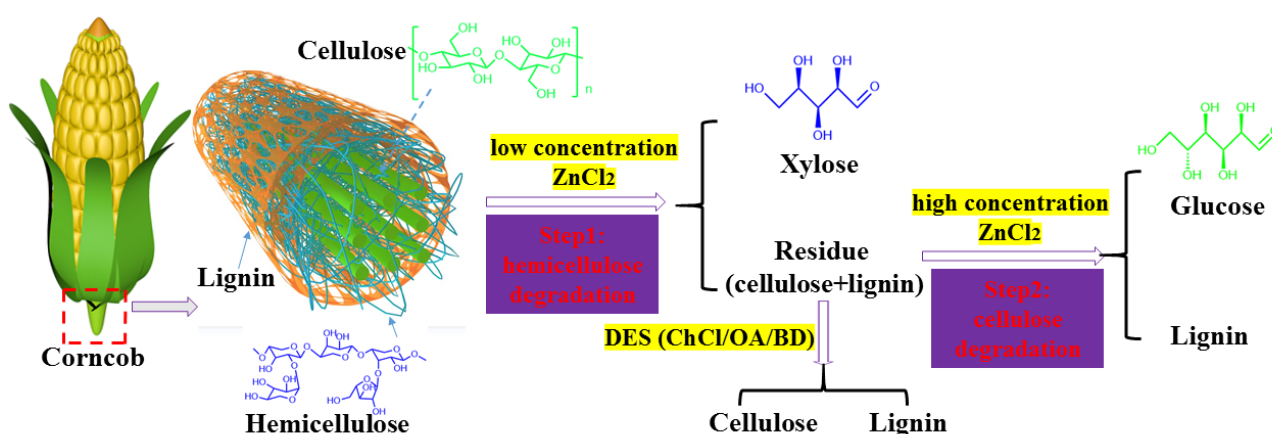
The unsustainability of coal, oil, and natural gas and their negative ecological and environmental impacts have forced many researchers to develop new processes based on renewable materials [1]. Lignocellulose biomass is the most common renewable carbon resource and has received much attention for its conversion into biofuels and other platform chemicals.

Cellulose, hemicellulose, and lignin are the three major components of lignocellulosic biomass. However, it is difficult to separate them by simple chemical or biological treatments due to their special complex structure [2,3]. In previous studies, compared with cellulose, hemicellulose has fewer hydrogen bonds and exposes more active centers for degradation [4–7]. Hemicellulose can be converted into xylose, xylitol, furfural, or other chemicals [8–10]. Cellulose is difficult to dissolve and process due to its crystal structure and complex hydrogen bonds [11–13]. However, cellulose, as a macromolecular polysaccharide, can still be degraded into oligosaccharides under certain conditions and continue to degrade glucose and 5-hydroxymethylfurfural [14–20]. Lignin is a complex class of aromatic phenolic polymers. Numerous literature reports on lignin extraction with deep eutectic solvent (DES) or organic solvents [21–23].

In the treatment of lignocellulose, inorganic saline solutions are commonly used [24]. Compared with organic solvents and ionic liquids, the inorganic saltwater solution has stable and low vapor pressure properties, which are safer, environmentally friendly, and clean [25–28]. Corncob is a lignocellulosic biomass of interest. It is often used as a raw material for biomass conversion because of its high hemicellulose, cellulose content, low price, and ease of obtaining [29–32].

Alkali, acid, hot water pretreatment, and enzymatic hydrolysis are common methods for treating and degrading biomass, but these methods have advantages and disadvantages. Alkaline systems can partially degrade carbohydrates and produce some phenolic derivatives [33]. Acidic treatment may cause an increase in by-products, such as furfural, furroic acid, and 5-HMF [34–36]. The enzymatic solution method is relatively mild and environmentally friendly but may be high-cost and limited in production [37,38]. Hot water pretreatment is economical and environmentally friendly but has a longer reaction time and low yield [39,40].

In this work, we performed the selective isolation of xylose and glucose in a very simple two-step method by adjusting the concentration of ZnCl_2 in the solution, using untreated corncob as the feedstock (Scheme 1). Firstly, corncob powder was treated with a lower concentration of ZnCl_2 to transfer the hemicellulose to xylose. Next, we separated the two solid-liquid phases to obtain a xylose-rich solution and a solid residue of cellulose and lignin. In the second step, a high-concentration of ZnCl_2 treatment transforms the cellulose from the remaining filter residue into glucose, resulting in a glucose-rich solution and residual solid of lignin. By adding ammonia aqueous solution or passing through ammonia gas to the filtrate, the Zn^{2+} ion can form insoluble complex precipitation after it is filtered and dried, converted into $\text{Zn}(\text{OH})_2$, and the zinc ion is recycled. Zn^{2+} ions can be recovered to 97.94% throughout the process. It provides a simple and efficient method of treating biomass to produce xylose, glucose, and lignin. Furthermore, for the solid residue of the first-step reaction, a ternary deep eutectic solvent (DES) (choline chloride/oxalic acid/1,4-butanediol, $\text{ChCl}/\text{OA}/\text{BD}$) has been used to separate the cellulose and lignin efficiently, and high-quality cellulose (Re-C) and lignin (Re-L) were obtained. It provides a simple method to disassemble the lignocellulose for monosaccharides, lignin, and cellulose. Compared with similar studies, simple and environment-friendly reagents were used in this work. The reaction conditions were mild (lower temperature, shorter reaction time), and the yields of xylose and glucose were higher [41–43].



Scheme 1. Schematic diagram of the degradation of corncob via an efficient two-step method or DES route.

2. Result and Discussion

2.1. Effect of ZnCl_2 Content

Here, corncob powder was treated directly with different concentrations of ZnCl_2 at $95\text{ }^\circ\text{C}$ for 10 min, and the yields of xylose and glucose were listed in Table 1. Interestingly,

the xylose and glucose yield strongly correlates with the concentration of $ZnCl_2$, as shown in Figure 1. At the lower concentration of $ZnCl_2$ (50 w% of solution), the main product is xylose, while the yield of glucose is relatively low. However, as the concentration of $ZnCl_2$ increases, the yield of xylose decreases while the yield of glucose gradually increases. This may be due to the concentration of $ZnCl_2$ related to the coordination of zinc ions with oxygen atoms on the hydroxyl group of the hemicellulose and cellulose [44,45], and the lower concentration of treatment can only degrade hemicellulose because there are fewer hydrogen bonds.

Table 1. Effect of $ZnCl_2$ content on xylose and glucose yield (one pot).

M($ZnCl_2$)/g	9	10	11	12	13	14	15	16
xylose (%)	27.2	30.1	28.5	27.4	24.6	22.9	21.7	21.1
glucose (%)	2.7	3.9	9.3	14.7	20.9	26.4	30.0	27.5
xylose and glucose (%)	29.9	34.0	37.8	42.1	45.5	48.3	51.7	48.6

95 °C, 10 min, 5 mL 2M HCl, deionized water, total mass was 20 g. when the mass of $ZnCl_2$ is 16 g, 4 mL 2M HCl, 1.5 g corncob, the denominator of yield is the total quality of corncob.

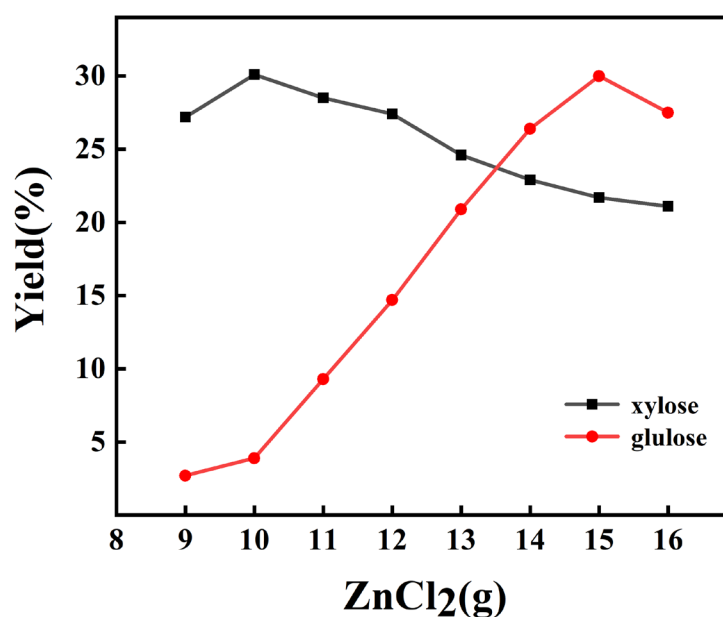


Figure 1. Effect of the concentration of $ZnCl_2$ on the yield of xylose and glucose (5 mL 2M HCl, ultrapure water, the total mass was 1.5 g).

Interestingly, due to many hydrogen bonds, cellulose has a dense crystalline region and was also degraded when treated at high concentrations (75 w% of solution). But as the treatment concentration continues to rise, the decrease of the yields of xylose and glucose may be due to the increased viscosity of the system, resulting in reduced mass transfer efficiency. Figure 2 shows the possible method for the formation of xylose and glucose by varying the concentration of $ZnCl_2$. In the first step, the lower concentration of $ZnCl_2$ converts hemicellulose into xylose (filtrate L1), while cellulose was better retained in R1. Next, at a high concentration of zinc chloride, the cellulose in R1 was degraded into glucose (L2), leaving the remaining lignin in the filter residue R2. Then, xylose in the filtration L1 was isolated as powder, while the solid R1 was furthermore treated by a DES for cellulose (Re-C) and lignin (Re-L) (Figure 3).

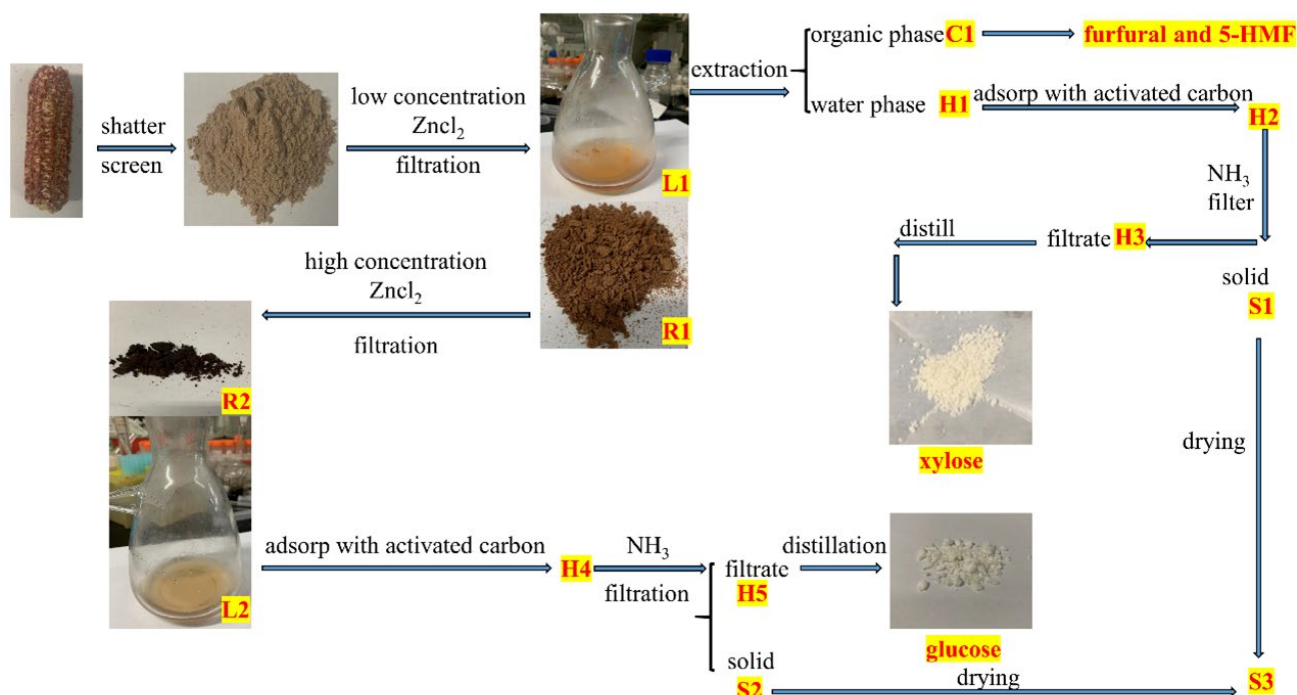


Figure 2. Corn cob decomposition into xylose and glucose with zinc chloride recovery.

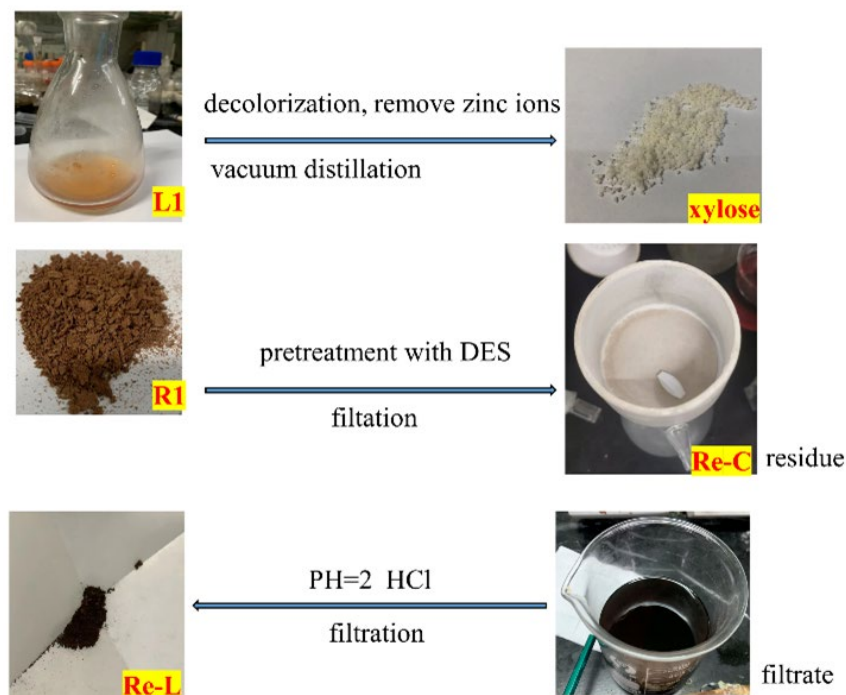


Figure 3. Fractionation of the solid residue of the first-step reaction to cellulose Re-C and lignin Re-L.

2.2. Effect of Temperature

The reaction temperature is crucial in this work, related to whether cellulose and hemicellulose can be hydrolysed. As shown in Tables 2 and 3, and Figure 4a,b, at room temperature, cellulose is difficult to hydrolysis even with a high concentration of acid and a long reaction time. But hemicellulose hydrolysis does not require a relatively high temperature and ZnCl_2 concentrations. At 65°C , treatment of the hemicellulose with the lower concentration yielded a considerable xylose yield (18.3 w%). However, with increasing temperature, the xylose production reaches the maximum of 30.4 w% at

95 °C. This may be because the side reaction is not intense at low temperatures. When the temperature is greater than 95 °C, then as the temperature continues to rise, we can observe that the product of the flask changes from light brown to black, indicating the degradation of monosaccharides or the formation of carbon dots [46,47].

Table 2. Effect of temperature on xylose and glucose yield in the first step.

Temperature/°C	65	75	85	95	105	115
xylose (%)	18.3	20.1	28.5	30.4	29.7	24.2
glucose (%)	1.6	1.9	2.4	3.6	3.4	2.9
xylose and glucose (%)	19.9	22.0	30.9	34.0	34.1	27.1

10 min, 5 mL 2M HCl, 5 mL deionized water, 10 g ZnCl₂, 1.5 g corncob, the denominator of yield is the total quality of corncob.

Table 3. Effect of temperature on xylose and glucose yield in the second step.

Temperature/°C	65	75	85	95	105	115
xylose (%)	3.5	3.3	2.7	2.6	2.4	2.2
glucose (%)	6.9	19.3	25.2	29.4	28.1	22.7
xylose and glucose (%)	10.4	22.6	27.9	32.0	30.5	24.9

10 min, 5 mL 2M HCl, 15 g ZnCl₂, R1, the denominator of yield is the total quality of corncob.

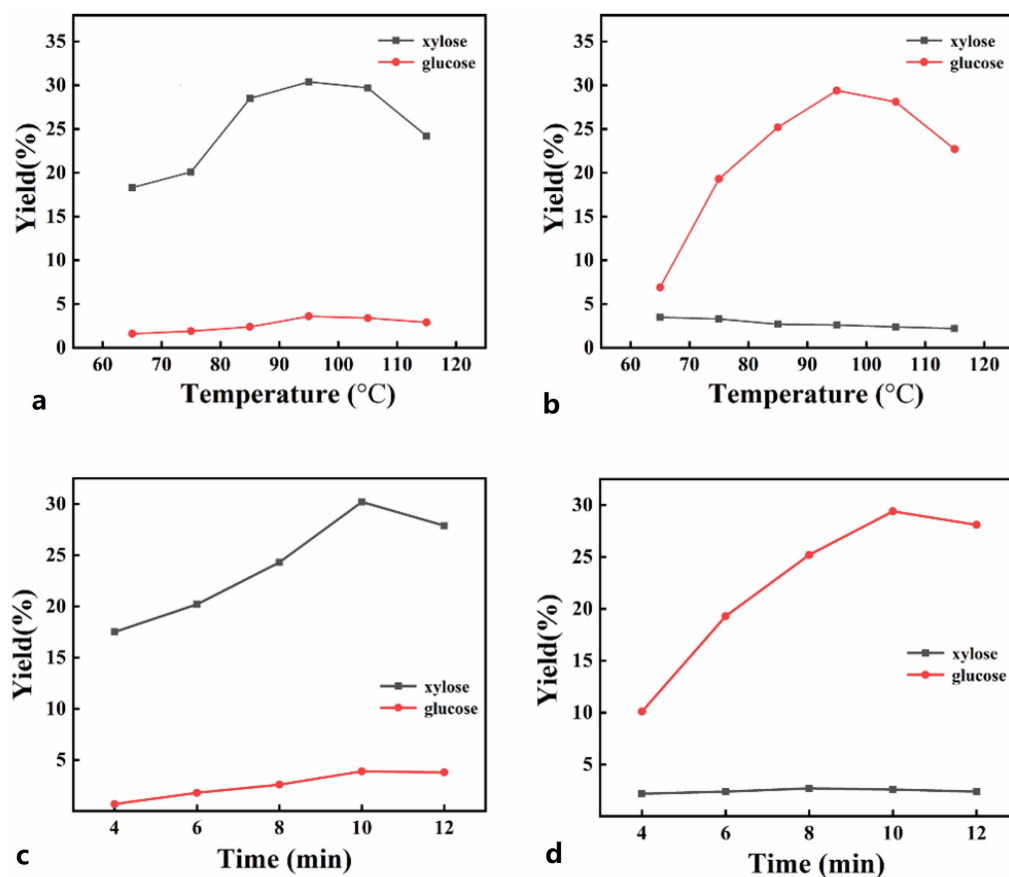


Figure 4. Effects of temperature on the (a) step-1 and (b) step-2 reactions. Effects of time on the (c) step-1 and (d) step-2 reactions.

Meanwhile, an increase in furfural as a byproduct was detected by HPLC. This indicates that the excessive temperature will accelerate the dehydration of the sugar, leading to the carbonization of the biomass and producing more humins. Interestingly, the low temperature did not convert the cellulose efficiently at high concentrations (65 °C, 6.9%), but the yield of glucose also peaked at 95 °C (29.4 w%). This may be due to the high concentration treatment having destroyed the cellulose structure, after which glucose production no longer requires high temperature. So in both low and high concentrations, we selected 95 °C as the reaction temperature.

It must be noted that due to the short reaction time, we need to preheat the reactants and the flask early. Otherwise, if following the conventional reaction method, the reactant has not been heated to the temperature of the oil bath when the reaction time ends. This situation will cause the reaction not to proceed effectively, and the yield is much reduced. Therefore, we mixed and stirred a certain mass of ZnCl₂ and corncob powder in a flask and next placed the flask in a 95 °C oil bath heater. We next measured the temperature of the in-bottle reactant with a thermometer. We quickly added hydrochloric acid and deionized water when 80 °C was reached and started the timing. At this point, the effects of dissolved heat and agitation will rapidly increase the temperature inside the flask to 93–95 °C and reach thermal equilibrium. Thus, the truth and accuracy of the reaction temperature are guaranteed.

2.3. Effect of Time

Reaction time is another key parameter; the results are shown in Tables 4 and 5. As shown in Figure 4c,d, when treated with lower concentrations of ZnCl₂, glucose yield was consistently low. It increased slowly over time due to the limited effect of Lewis acid on cellulose. However, the lower concentration treatment affects hemicellulose much more strongly and can be significantly converted into xylose in a short time (4 min, 17.5 w%). Therefore, the xylose yield was maximized at the reaction time of 10 min. At high concentrations of treatment, xylose yield was at low levels because hemicellulose had been removed, while glucose production also decreased after reaching a maximum. It may be because the long reaction time aggravates sugar dehydration and carbonization. To achieve a satisfactory separation effect and a maximum sugar yield, the low and high concentrations were treated with 10 min as the reaction time. Combining the two steps, the total yield of xylose is 97%, while glucose is 95%.

Table 4. Effect of time on xylose and glucose yield in the first step.

Time/min	4	6	8	10	12
xylose (%)	17.5	20.2	24.3	30.2	27.9
glucose (%)	0.7	1.8	2.6	3.9	3.8
xylose and glucose (%)	18.2	22.0	26.9	34.1	31.7

95 °C, 5 mL 2M HCl, 5 mL deionized water, 10 g ZnCl₂, 1.5 g corncob, the denominator of yield is the total quality of corncob.

Table 5. Effect of time on xylose and glucose yield in the second step.

Time/min	4	6	8	10	12
xylose (%)	2.2	2.4	2.7	2.6	2.4
glucose (%)	10.1	19.3	25.2	29.4	28.1
xylose and glucose (%)	12.3	21.7	27.9	33.0	30.5

95 °C, 5 mL 2M HCl, 15 g ZnCl₂, R1, the denominator of yield is the total quality of corncob.

2.4. Characterization of the Intermediates

The shape and microstructure change of the corncob during the two-step treatment were measured by means of SEM. As shown in Figure 5, in the images of the Corncob, we can see the packing of the irregular shapes, which is due to the hemicellulose, cellulose, and lignin being entangled with each other. However, after ZnCl_2 treatments, in the SEM images of R1 (Figure 5b–d), the apparent axial rod-shaped arrangement can be observed at all scales. This morphology is the characteristic crystal structure of cellulose. The cellulose structure in R1 is not well disrupted. However, in R2 (Figure 5e,f), we only observed an irregular porous structure, the remaining lignin, after removing the cellulose. This evidence confirmed that we achieved the purpose of isolating biomass and separate extraction of xylose and glucose, and lignin was also obtained simultaneously.

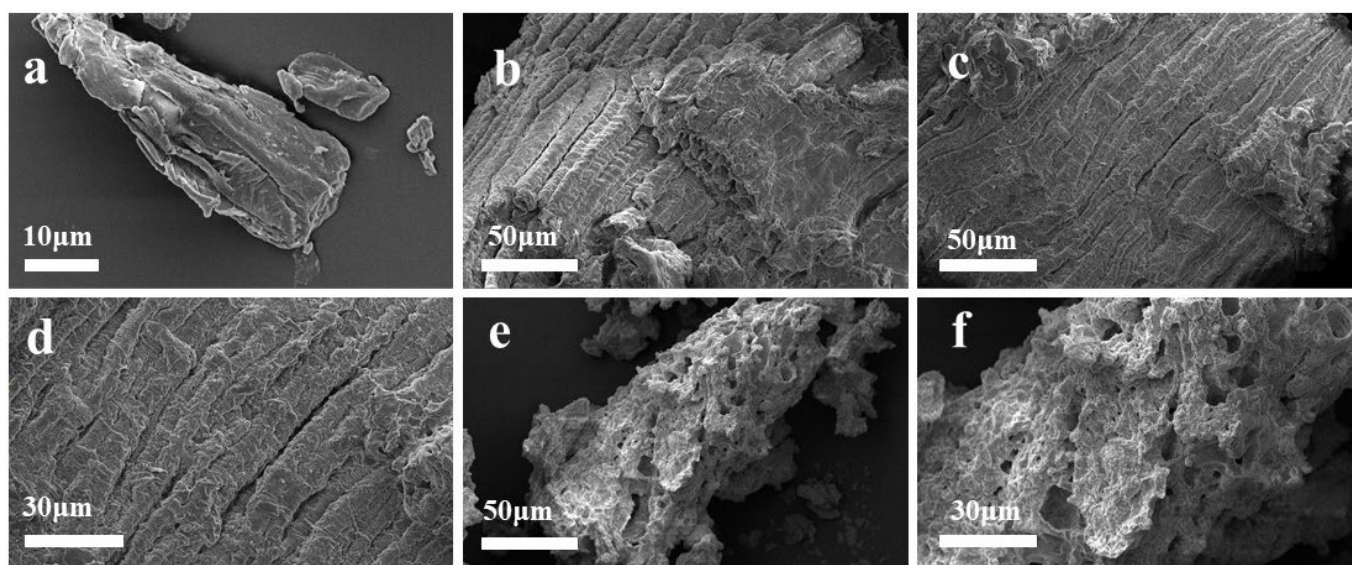


Figure 5. SEM images of the feedstock corncob (a), R1 (b–d), and R2 (e,f).

The FT-IR characterization was performed for the MCC, Corncob, R1, and R2, as shown in Figure 6a. At 3570 cm^{-1} , R2 signals much stronger than R1 and corncob because of the characteristic absorption of the phenolic hydroxyl group of the benzene ring in the lignin structure. Because the continuous two-step reaction removed the main components of hemicellulose and cellulose, the amount of lignin content in the second filter residue R2 was increased, so the characteristics of lignin were more obvious. Similarly, at 1609 cm^{-1} , it is also a significant signal for R2, the standard absorption peak for the vibration of the benzene ring skeleton in lignin. The peak at 1036 cm^{-1} is due to the stretching vibration of C-O in the polysaccharide. Since almost all of the polysaccharide in R2 has been transformed, the signal for this peak in R2 is somewhat weaker than that in R1 and Corncob. The peaks at 2918 cm^{-1} are generated by C-H extension vibrations in cellulose, shown in the MCC, Corncob, and R1 FTIR spectra. The cellulose has been removed in R2, so this signal is not obvious in the figure [48–50].

Figure 6b shows the XRD patterns of MCC, corncob, R1, and R2. They all had signals at the characteristic position of the cellulose ($2\theta = 22.4^\circ$), and the crystallinity (CrI) was 61.71%, 42.01%, and 54.13%, respectively, and the signal was insignificant in R2 [51,52]. This indicates that the lower concentration treatment can effectively remove the hemicellulose and retain the cellulose while the CrI of the cellulose also increases (from 42.01% to 54.13%). No obvious characteristic cellulose absorption peak in R2 occurs because the high concentration of treatment degraded the cellulose into glucose, as confirmed by HPLC.

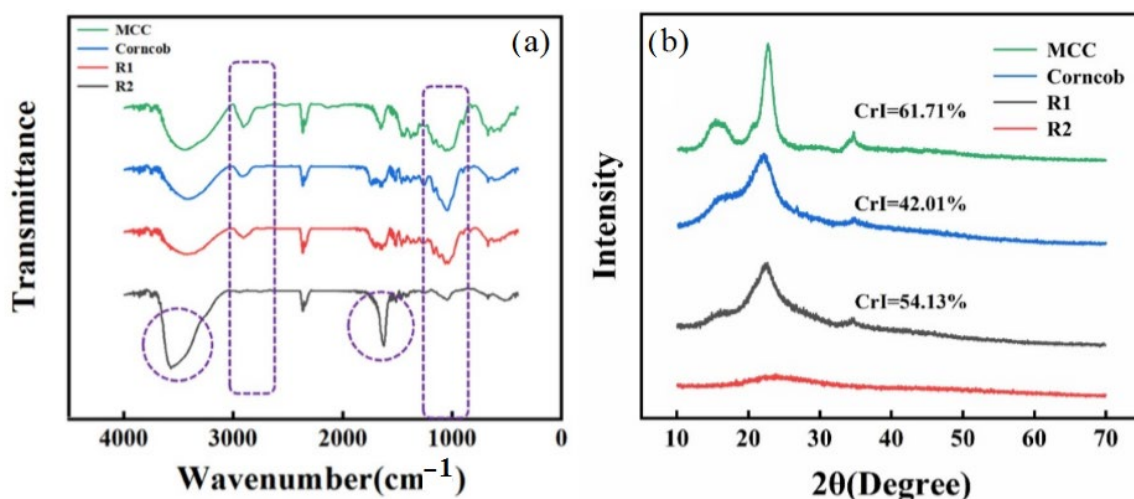


Figure 6. (a) FTIR and (b) XRD spectra of MCC, corncob, R1, and R2.

2.5. Recovery of Zinc Ions

We used the coordination of Zn^{2+} and NH_4^+ to separate and recover the Zn^{2+} ion [53]. In this system, an ammonia aqueous solution or ammonia gas was added, and Zn^{2+} and NH_4^+ could combine to form a complex and an insoluble complex. S1 and S2 are obtained in a filtered manner, and S1 S2 is heated and dried and converted to S3. XRD studies reveal that the main component of S3 is $Zn(OH)_2$ (Figure 7). S3, $Zn(OH)_2$, and a mixture of both showed highly similar features on the XRD profile. Each absorption peak on the graph line of $Zn(OH)_2$ can correspond to the same position in S3, which indicates the high purity of the main component $Zn(OH)_2$ in S3. In addition, in the XRD patterns, the $Zn(OH)_2$ and S3 graph lines only differ at $2\theta = 8.1^\circ$, which may be due to the anisotropy.

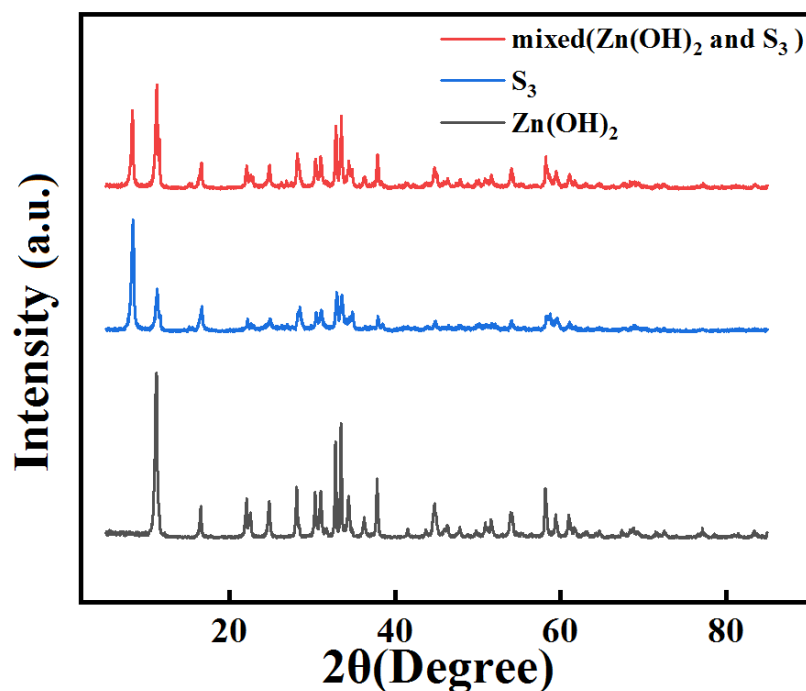


Figure 7. XRD patterns of $Zn(OH)_2$, S_3 , and the mixture of $Zn(OH)_2$ and S_3 .

The precipitation mode of feeding through ammonia gas and adding ammonia water had a similar effect, obtaining $R(Zn^{2+}) = 97.94\%$ and $R(Zn^{2+}) = 96.71\%$, respectively, probably because the ammonia water introduced more solvents, and the quality of the

precipitation was reduced. Notably, although precipitation occurs immediately after the addition of the reagent, placing the filtrate for a longer time is also necessary (in a 50 mL glass beaker for more than 24 h). According to the principle of precipitation dissolution equilibrium, precipitation of the filtrate several times can reduce the concentration of Zn^{2+} in the liquid and improve $R(Zn^{2+})$.

In addition, the residual Zn^{2+} ion in the as-prepared xylose and glucose were also measured by means of ICP. They are 119.44 mg/L and 64.61 mg/L, respectively. The calculated purity of xylose was 98.96%, and that of glucose was 99.41%.

2.6. The Formation of Lignin-R2

The R1, obtained by the lower concentration treatment, mainly comprises cellulose and lignin. After R1 was treated by step 2, most of the cellulose was degraded, and the residue should be lignin. The NMR (HSQC) studies were carried out to analyze its purity. For the 1H - ^{13}C HSQC NMR spectroscopy using a Bruker AVIII 400 MHz spectrometer equipped with a DCH cryoprobe, around 50 mg of Re-L or R2 was dissolved in 1.2 mL of DMSO- d_6 . The spectral widths were 12 ppm (11 to 1 ppm) and 220 ppm (from 200 to 20 ppm) for the 1H and ^{13}C dimensions, respectively. The peak of the solvent (DMSO- d_6) was used as a reference point for the internal chemical shift. Data of spectra were processed using standard MestReNova-NMR2010 software.

Figure 8 shows the 1H - ^{13}C HSQC NMR spectrum of the as-obtained R2, and many hydroxyl corresponding signals are displayed. The signals are mainly aromatic region signals corresponding to guaiacyl (G), *p*-hydroxyphenyl (H), and syringyl (S) units of lignin. The side chains in the HSQC map are located in ($\delta C/\delta H$ 50–95/2.8–4.5 ppm), and the aromatic regions are located in ($\delta C/\delta H$ 100–135/6.2–7.8 ppm). The signal at $\delta C/\delta H$ 55.65/3.83 ppm corresponds to the methoxy group and several β -O-4' aromatic ether bonds. In the spectrograph, the main position of the C_α - H_α bonds of the A units connected to the G units and S units, respectively, is located in $\delta C/\delta H$ 65.18/4.12 and 66.73/4.24 ppm. The C_γ - H_γ correlations in structures A, B, and C can be distinguished at $\delta C/\delta H$ 60.30/3.54, 60.59/3.41, 67.42/3.39 ppm, respectively. The signal of the C_β - H_β bond between structures B and C overlaps with that of the methoxy group, which are located in $\delta C/\delta H$ 54.67/3.44 and 53.63/3.10 ppm, respectively. The $C_{2,6}$ - $H_{2,6}$ bonds of the S' unit are mainly at $\delta C/\delta H$ 111.14/7.11 ppm position, which is a relatively weak signal. The C_5 - H_5 and C_6 - H_6 bonds of the G structural unit were observed at $\delta C/\delta H$ 116.22/6.90 and 116.12/6.79 ppm positions, respectively. Furthermore, the peaks of $C_{2,6}$ - $H_{2,6}$ and $C_{3,5}$ - $H_{3,5}$ bonds of the H structural unit were observed at $\delta C/\delta H$ 115.38/6.63 and 130.80/7.53 ppm positions. The above observations indicate that the obtained R2 has characteristic structures and bonds of lignin, with main components of lignin.

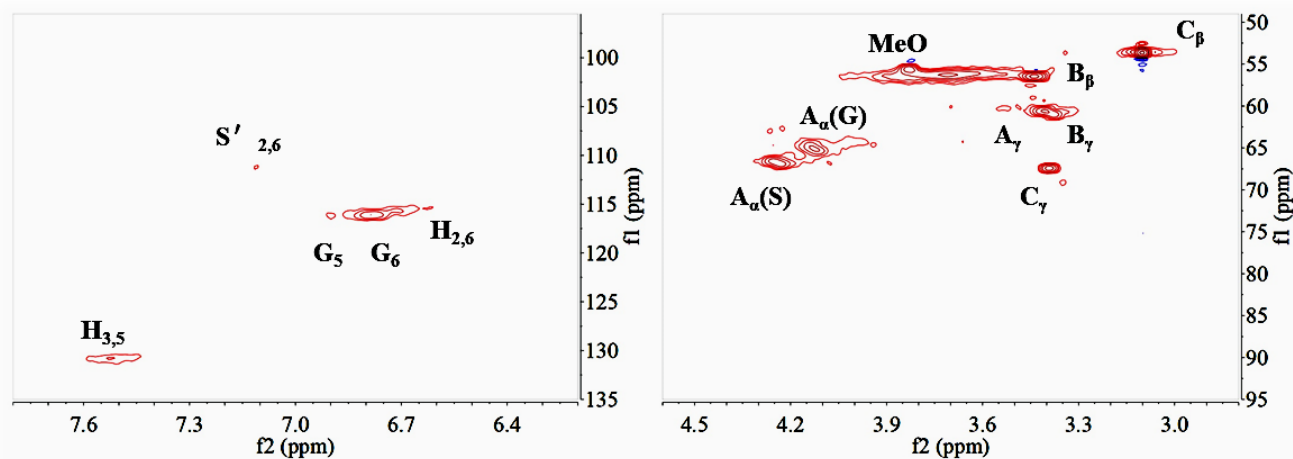


Figure 8. 1H - ^{13}C heteronuclear single quantum correlation (HSQC) NMR spectroscopy of R2.

2.7. The Formation of Re-C and Re-L

R1 can be treated by DES to yield cellulose Re-C and lignin Re-L, respectively. Next, we performed an XRD characterization (Figure 9) of Re-C, and Re-C has cellulose-characteristic absorption peaks at $2\theta = 22.4^\circ$. In addition, the crystallinity of the Re-C (53.69%) was significantly higher than that of the corn cob (42.01%) and was similar to that of the filter residue R1 (54.13%). This indicates that the lower concentration treatment selectively degraded hemicellulose and well-preserved the structure of cellulose. Moreover, the method provides new ideas and insights into the selective separation of lignocellulose.

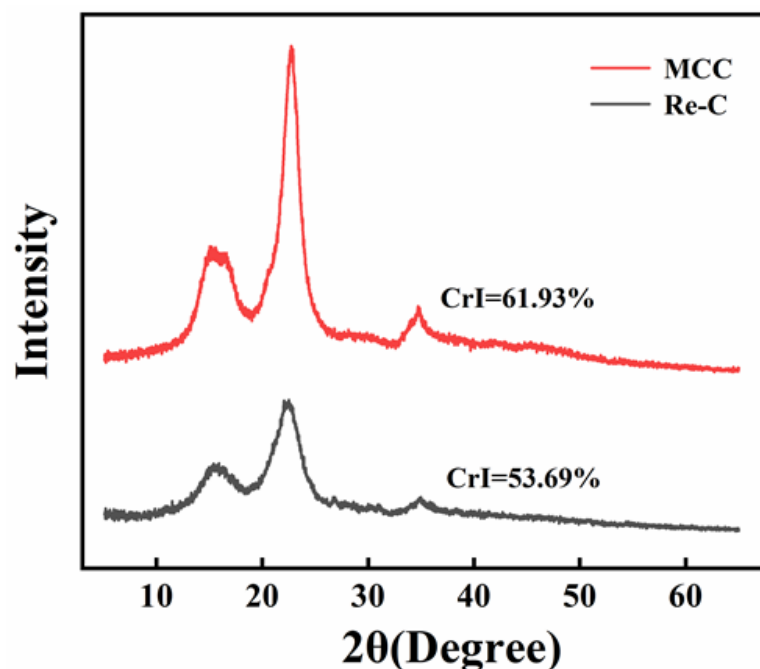


Figure 9. XRD spectra of MCC and Re-C.

Figure 10 shows the ^1H - ^{13}C HSQC NMR spectrum of the Re-L. It also shows the typical structural feature of lignin, similar to R2. (the method is the same as Section 2.7)

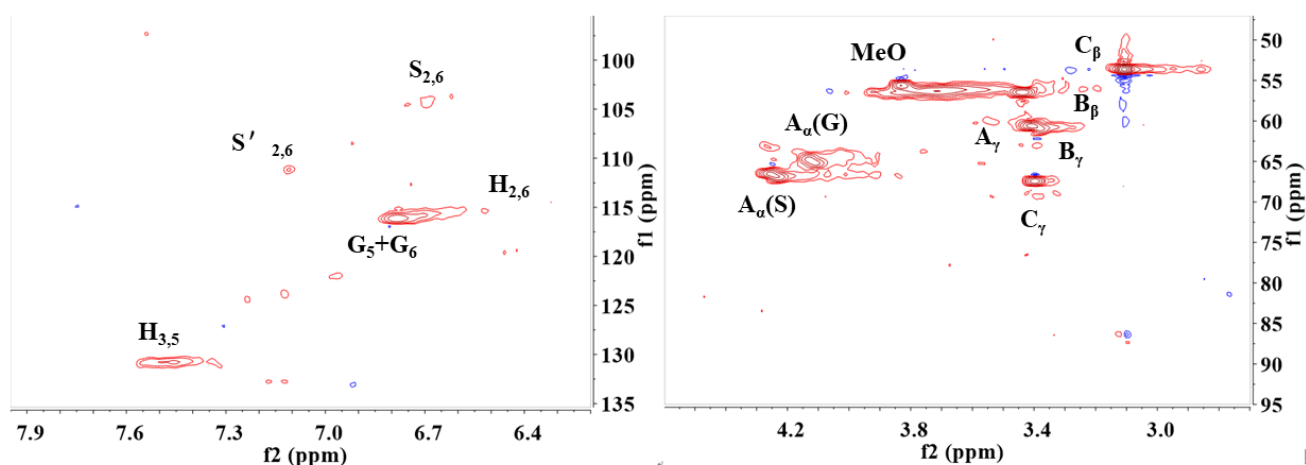


Figure 10. ^1H - ^{13}C heteronuclear single quantum correlation (HSQC) NMR spectroscopy of Re-L.

Interestingly, a clear distinction is shown between them, with a clear signal of $\text{C}_{2,6}$ - $\text{H}_{2,6}$ bonds of the S unit located in $\delta\text{C}/\delta\text{H}$ 103.93/6.69 ppm, appearing in Re-L, but not in R2. This distinction may be due to conditional differences between the two reactions. Moreover, the spectra of Re-L also showed structural information of lignin, demonstrating the lignin

purity. The signal at $\delta C/\delta H$ 56.18/3.84 ppm corresponds to the methoxy group and several β -O-4' aromatic ether bonds. In the spectrograph, the main position of the C_α - H_α bonds of the A units connected to the G units and S units, respectively, is located in $\delta C/\delta H$ 65.10/4.11 and 66.55/4.25 ppm. The C_γ - H_γ correlations in structures A, B, and C can be distinguished at $\delta C/\delta H$ 60.65/3.41, 62.18/3.39, 67.32/3.40 ppm, respectively. The signal of the C_β - H_β bond between structures B and C overlaps with that of the methoxy group, which are located in $\delta C/\delta H$ 53.62/3.11 and 54.67/3.44 ppm, respectively. The $C_{2,6}$ - $H_{2,6}$ bonds of the S' unit are mainly at $\delta C/\delta H$ 111.12/7.11 ppm. The C_5 - H_5 and C_6 - H_6 bonds of the G structural unit were observed at $\delta C/\delta H$ 116.12/6.78 and 115.16/6.78 ppm positions, respectively. Furthermore, the peaks of $C_{2,6}$ - $H_{2,6}$ and $C_{3,5}$ - $H_{3,5}$ bonds of the H structural unit were observed at $\delta C/\delta H$ 115.39/6.52 and 130.79/7.46 ppm positions.

According to Figure 11, in the whole process, we obtained more than 60 w% of the monosaccharides (xylose and glucose), which is an exciting thing. At the same time, xylose and glucose get a good separation effect. Furthermore, in the final product, we obtained 15.3 w% of the lignin, enabling the efficient utilization of the lignocellulose. In addition, the solid residue of the first-step reaction can also be efficiently fractionated into high-quality cellulose and lignin by means of a ternary DES system.

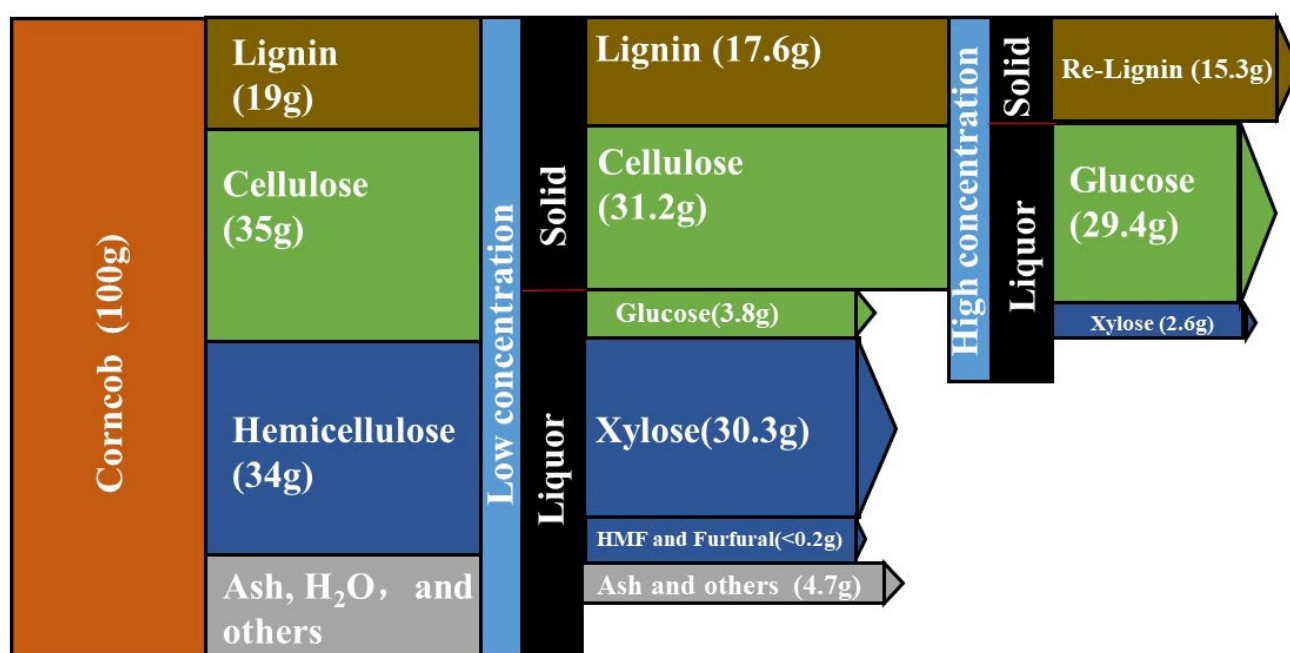


Figure 11. Mass balance flow diagram.

3. Materials and Methods

3.1. Materials

Corncob from Inner Mongolia, China, were placed in sealed plastic bags to dry naturally for about three months, ground to powder, and screened through 80 mesh before being used. The weight loss of corncob powder was less than 0.01 g/g in three months. The main components of the corncob were determined by the NREL LAP method, resulting in 35% cellulose content, 34% hemicellulose content, and 19% lignin content.

Anhydrous zinc chloride, concentrated hydrochloric acid (12 mol/L), aqueous ammonia (25–28 w%), ethyl acetate, choline chloride, oxalate dihydrate, 1,4-butanediol, glucose, xylose, furfural, 5-HMF were all purchased from Sinopharm Chemical Reagents Co., LTD. (Shanghai, China). Microcrystalline cellulose, purchased from Shanghai Aladdin reagent company (Shanghai, China). Ammonia gas, analytical pure, purchased from Anhui Hefei Hengxing Industrial Gas Co., Ltd. (Hefei, China), stored in cylinders. The flow rate is 1 mL/s.

Chromatographic grade acetonitrile for HPLC was purchased from Merck (Rahway, NJ, USA). Ultrapure water was prepared via a Milli-Q system (18.2 M Ω , Millipore, Burlington, MA, USA). The hydrochloric acid (2 mol/L) used in the experiment was obtained by diluting the concentrated hydrochloric acid and ultrapure water.

3.2. Selective Degradation of Hemicellulose: Lower Concentration ZnCl₂ Solution Treatment

10 g of anhydrous zinc chloride was put in a 50 mL flask, and then 1.5 g of crushed corncob powder was added under magnetical stirring to mix them evenly. Next, the mixture was heated by a water bath with a set temperature of 95 °C. The temperature of the reactant in the flask was measured using a thermometer. When the temperature of the reactant reached 80 °C, 5 mL of ultrapure water and 5 mL of hydrochloric acid (2 mol/L) were added under stirring and maintaining the reaction temperature at 90–95 °C using the dissolved heat of zinc chloride. The timing was started after the addition of water and hydrochloric acid was completed. After 10 min of the reaction, the flask was removed from the heater, and 30 mL of cold ultrapure water was added to stop the reaction. The products inside the flask were filtered to generate residue R1 and filtrate L1, respectively. The L1 components were determined by HPLC (Shimadzu, LC-20D). Byproduct species was determined by adding 20 mL of ethyl acetate to extract L1, resting for 2 h, and detecting the organic phase C1 by the HPLC method. Then 0.5 g activated carbon was added to the aqueous phase H1 for adsorption of pigment from corn cob and decolorization, under stirring at 65 °C for 0.5 h. Next, it was filtered to obtain the filtrate H2. Ammonia was injected into H2 to adjust pH = 8 to allow the zinc ions to precipitate. Three repeats were carried out to completely remove the zinc ions in H2. The filter residue S1 and the xylose-rich filtrate H3 were treated separately, and the H3 was distilled under reduced pressure to remove the water, and the resulting white solid was the xylose.

3.3. Selective Degradation of Cellulose: High Concentration ZnCl₂ Solution Treatment

15 g of anhydrous zinc chloride was added in a 50 mL flask, and then add the crushed and dried residue R1, and mixed under magnetic stirring at room temperature. The mixture was heated by a water bath with a set temperature of 95 °C. The temperature of the reactant in the flask was measured using a thermometer. When the temperature of the reactant reached 80 °C, 5 mL of hydrochloric acid (2 mol/L) was added with a pipette gun under stirring, and maintain the reaction temperature at 90–95 °C using the dissolved heat of zinc chloride. The timing was started after the addition of hydrochloric acid was completed, and after 10 min of the reaction, the flask was removed from the heater, and 30 mL of cold ultrapure water was added to stop the reaction. The products inside the flask were filtered to generate residue R2 and filtrate L2, respectively. The L2 components were determined by HPLC. The 0.5 g activated carbon was added to the aqueous phase L2 for adsorption of pigment from corn cob and decolorization, heated, and stirred at 65 °C for 0.5 h, and it was filtered to obtain the filtrate H4. Ammonia was injected into H4 to adjust pH = 8 to allow zinc ions to precipitate and filter. The process was repeated three times to completely remove the zinc ions in H4. The filter residue S2 and the glucose-rich filtrate H5 were treated separately, and the H5 was distilled under reduced pressure to remove the water, and the resulting white solid was the glucose.

3.4. Fractionation of Lignocellulose in DES

The solid residue of the first-step reaction is a complex of cellulose and lignin, which can be fractionated using the green solvent of DES [54]. Here, a ternary DES of oxalic acid dihydrate (OA, 0.1 mol), choline chloride (ChCl, 0.1 mol), and 1,4-butanediol (BD, 0.2 mol) were prepared and was used as the solvent to separate the solid residue in an oil bath at 110 °C for 5 h under continuous stirring. After the reaction, the mixture was added to 100 mL of anti-solvent (ethanol:water = 3:7) under stirring for 2 h. The filter residues were washed thrice with 100 mL anti-solvent and dried to obtain cellulose Re-C. Then, ethanol in the

filtrate was removed by rotary evaporation, and the filtrate was precipitated in 100 mL of dilute hydrochloric acid (pH = 2) to obtain lignin Re-L.

3.5. Method of Recovery of Zinc Ion

The residues S1 and S2 were dried in the vacuum drying chamber for 24 h at a temperature of 80 °C. The dried white solid S3 is insoluble in water, which was measured by XRD. Its XRD profile is the same as that of Zn(OH)₂, indicating that the main component of S3 is Zn(OH)₂. Then, S3 was weighed to calculate the zinc ion recovery.

3.6. Residual Zinc Ions in the Products

The residual zinc ion in xylose and glucose were detected using an Inductively coupled plasma spectrometer (ICP), model number PerkinElmer Optima 7300 DV. The obtained xylose and glucose were dissolved in ultrapure water and fixed to 50 mL.

3.7. Calculation Method of the Parameters

The selectivity of xylose: $S_x = Y_{mxi} / (Y_{mxi} + Y_{mgi})$, and the selectivity of glucose: $S_x = Y_{mgi} / (Y_{mxi} + Y_{mgi})$, where $I = 1$ or 2 , indicates the first step and second step, m is the relative mass, while m_1 , m_2 , and m_3 are the mass of corncob, hemicellulose, and cellulose. The crystallinity (crystallinity index, CrI) of corncob, MCC, R1, and R2:

$$\text{CrI} = \frac{I_{002} - I_{am}}{I_{002}}$$

where I_{002} is the intensity of the diffraction peak at $2\theta = 22.4^\circ$, and I_{am} represents the amorphous portion at $2\theta = 18^\circ$.

3.8. SEM Characterization of Corncob and R1, R2

The microstructure of products was observed by scanning electron microscope (SEM, Gemini SEM 500). Before testing, products were replaced with water and then freeze-dried.

3.9. FT-IR Characterization of Corncob, MCC, R1, and R2

Fourier transforms infrared (FTIR) spectra were recorded on a Bruker vector-2 spectrophotometer in the 400–4000 cm^{-1} .

3.10. XRD Characterization of Corncob, MCC, R1, and R2

XRD analysis was performed on a Philips X' Pert PRO SUPER X-ray diffractometer with Cu K α radiation ($\lambda = 1.54056 \text{ \AA}$).

3.11. Determination of Xylose and Glucose in the Filtrate L1 and L2 by Means of HPLC

Monosaccharides in the filtrates were quantitatively analyzed by means of high-performance liquid chromatography (Shimadzu) equipped with a refractive index detector (RID-10A) and NH₂ column ($4.6 \times 250 \text{ mm}^2$, purchased from Agilent, 880952-708) at 40 °C. The mixed solution of acetonitrile and deionized water (70:30 v/v) was used as the mobile phase at a flow rate of 1.0 mL min^{-1} .

3.12. Determination of Furfural and 5-HMF in the C1 by Means of HPLC

The dehydration products (5-HMF and furfural) of the monosaccharides were determined using HPLC (Shimadzu) with a C18 column ($4.6 \times 250 \text{ mm}^2$, purchased from Agilent) at 40 °C and a UV-vis detector (SPD-20A) at 210 nm. The mixed methanol and ultrapure water (30:70, v/v) were used as the mobile phase at a flow rate of 0.7 mL min^{-1} . Due to the low content, only furfural and 5-HMF were qualitatively examined in this work.

3.13. The XRD Characterization of Recovered Zn(OH)₂

XRD analysis was performed on a Philips X'Pert PRO SUPER X-ray diffractometer with Cu K α radiation ($\lambda = 1.54056 \text{ \AA}$). Using the XRD method to detect the recovered Zn(OH)₂ and the standard Zn(OH)₂.

4. Conclusions

Degradation of lignocellulosic biomass is a key step to disassembling the complex structure of lignocellulose. Here, the lower concentration of ZnCl₂ aqueous solution (30–55 wt %) was an efficient system to degrade hemicellulose to xylose (97%) selectively. At the same time, cellulose and lignin have less change. The selective degradation of hemicellulose makes the lignocellulose easier to degrade or fraction. For degradation, a high glucose yield (95%) can be achieved using a high concentration of ZnCl₂ aqueous solution. In contrast, high-quality cellulose can be isolated when a ternary DES (ChCl/OA/BD) system is used. At the same time, higher purity lignin can be obtained by both treatment methods. It provides a new idea and route for the efficient separation and utilization of lignocellulosic biomass.

Author Contributions: Conceptualization, L.Y.; Methodology, C.T.; Validation, X.L.; Investigation, S.Z. and Y.D.; Resources, H.Q. and X.Y.; Data curation, H.L. All authors have read and agreed to the published version of the manuscript.

Funding: This work is supported by the National Key R&D Program of China (No. 2020YFA0710700), the National Natural Science Foundation of China (No. 51873201), and the Fundamental Research Funds for the Central Universities (No. YD2060002015).

Institutional Review Board Statement: Not applicable.

Informed Consent Statement: Not applicable.

Data Availability Statement: Data are available from the authors if required.

Conflicts of Interest: The authors declare no conflict of interest.

Sample Availability: Not applicable.

References

1. Zhou, C.H.; Xia, X.; Lin, C.X.; Tong, D.S.; Beltramini, J. Catalytic conversion of lignocellulosic biomass to fine chemicals and fuels. *Chem. Soc. Rev.* **2011**, *40*, 5588–5617. [[CrossRef](#)]
2. Scapini, T.; Dos Santos, M.S.N.; Bonatto, C.; Wancura, J.H.C.; Mulinari, J.; Camargo, A.F.; Klanovicz, N.; Zabet, G.L.; Tres, M.V.; Fongaro, G.; et al. Hydrothermal pretreatment of lignocellulosic biomass for hemicellulose recovery. *Bioresour. Technol.* **2021**, *342*, 126033. [[CrossRef](#)]
3. Liu, Y.; Sun, B.; Zheng, X.; Yu, L.; Li, J. Integrated microwave and alkaline treatment for the separation between hemicelluloses and cellulose from cellulosic fibers. *Bioresour. Technol.* **2018**, *247*, 859–863. [[CrossRef](#)]
4. Jiang, Z.; Budarin, V.L.; Fan, J.; Remón, J.; Li, T.; Hu, C.; Clark, J.H. Sodium Chloride-Assisted Depolymerization of Xylo-oligomers to Xylose. *ACS Sustain. Chem. Eng.* **2018**, *6*, 4098–4104. [[CrossRef](#)]
5. Zhou, X.; Li, W.; Mabon, R.; Broadbelt, L.J. A mechanistic model of fast pyrolysis of hemicellulose. *Energy Environ. Sci.* **2018**, *11*, 1240–1260. [[CrossRef](#)]
6. Ding, J.; Yoo, C.G.; Pu, Y.; Meng, X.; Bhagia, S.; Yu, C.; Ragauskas, A.J. Cellulolytic enzyme-aided extraction of hemicellulose from switchgrass and its characteristics. *Green Chem.* **2019**, *21*, 3902–3910. [[CrossRef](#)]
7. Hernandez-Perez, A.F.; Costa, I.A.; Silva, D.D.; Dussan, K.J.; Villela, T.R.; Canetti, E.V.; Carvalho, J.A., Jr.; Soares Neto, T.G.; Felipe, M.G. Biochemical conversion of sugarcane straw hemicellulosic hydrolyzate supplemented with co-substrates for xylitol production. *Bioresour. Technol.* **2016**, *200*, 1085–1088. [[CrossRef](#)]
8. Cai, C.M.; Zhang, T.; Kumar, R.; Wyman, C.E. Integrated furfural production as a renewable fuel and chemical platform from lignocellulosic biomass. *J. Chem. Technol. Biotechnol.* **2014**, *89*, 2–10. [[CrossRef](#)]
9. Monteiro, C.R.M.; Avila, P.F.; Pereira, M.A.F.; Pereira, G.N.; Bordignon, S.E.; Zanella, E.; Stambuk, B.U.; de Oliveira, D.; Goldbeck, R.; Poletto, P. Hydrothermal treatment on depolymerization of hemicellulose of mango seed shell for the production of xylooligosaccharides. *Carbohydr. Polym.* **2021**, *253*, 117274. [[CrossRef](#)]
10. Perez, R.F.; Fraga, M.A. Hemicellulose-derived chemicals: One-step production of furfuryl alcohol from xylose. *Green Chem.* **2014**, *16*, 3942–3950. [[CrossRef](#)]

11. Kuzmina, O.; Bhardwaj, J.; Vincent, S.R.; Wanasekara, N.D.; Kalossaka, L.M.; Griffith, J.; Potthast, A.; Rahatekar, S.; Eichhorn, S.J.; Welton, T. Superbase ionic liquids for effective cellulose processing from dissolution to carbonization. *Green Chem.* **2017**, *19*, 5949–5957. [[CrossRef](#)]
12. FitzPatrick, M.; Champagne, P.; Cunningham, M.F.; Whitney, R.A. A biorefinery processing perspective: Treatment of lignocellulosic materials for the production of value-added products. *Bioresour. Technol.* **2010**, *101*, 8915–8922. [[CrossRef](#)]
13. Ghasemi, M.; Tsianou, M.; Alexandridis, P. Assessment of solvents for cellulose dissolution. *Bioresour. Technol.* **2017**, *228*, 330–338. [[CrossRef](#)]
14. Liu, Z.; Li, L.; Liu, C.; Xu, A. Saccharification of cellulose in the ionic liquids and glucose recovery. *Renew. Energy* **2017**, *106*, 99–102. [[CrossRef](#)]
15. Wu, T.; Li, N.; Pan, X.; Chen, S.-L. Homogenous hydrolysis of cellulose to glucose in an inorganic ionic liquid catalyzed by zeolites. *Cellulose* **2020**, *27*, 9201–9215. [[CrossRef](#)]
16. Sixta, H.; Michud, A.; Hauru, L.; Asaadi, S.; Ma, Y.; King AW, T.; Kilpeläinen, I.; Hummel, M. Ioncell-F: A high-strength regenerated cellulose fibre. *Nordic Pulp Paper Res. J.* **2015**, *30*, 43–57. [[CrossRef](#)]
17. Li, Z.; Su, K.; Ren, J.; Yang, D.; Cheng, B.; Kim, C.K.; Yao, X. Direct catalytic conversion of glucose and cellulose. *Green Chem.* **2018**, *20*, 863–872. [[CrossRef](#)]
18. Yan, L.; Ma, R.; Wei, H.; Li, L.; Zou, B.; Xu, Y. Ruthenium trichloride catalyzed conversion of cellulose into 5-hydroxymethylfurfural in biphasic system. *Bioresour. Technol.* **2019**, *279*, 84–91. [[CrossRef](#)]
19. Wu, Q.; Zhang, G.; Gao, M.; Cao, S.; Li, L.; Liu, S.; Xie, C.; Huang, L.; Yu, S.; Ragauskas, A.J. Clean production of 5-hydroxymethylfurfural from cellulose using a hydrothermal/biomass-based carbon catalyst. *J. Clean. Prod.* **2019**, *213*, 1096–1102. [[CrossRef](#)]
20. Wang, J.; Xi, J.; Wang, Y. Recent advances in the catalytic production of glucose from lignocellulosic biomass. *Green Chem.* **2015**, *17*, 737–751. [[CrossRef](#)]
21. Sadeghifar, H.; Ragauskas, A. Perspective on Technical Lignin Fractionation. *ACS Sustain. Chem. Eng.* **2020**, *8*, 8086–8101. [[CrossRef](#)]
22. Yoo, C.G.; Meng, X.; Pu, Y.; Ragauskas, A.J. The critical role of lignin in lignocellulosic biomass conversion and recent pretreatment strategies: A comprehensive review. *Bioresour. Technol.* **2020**, *301*, 122784. [[CrossRef](#)]
23. Xia, Q.; Liu, Y.; Meng, J.; Cheng, W.; Chen, W.; Liu, S.; Liu, Y.; Li, J.; Yu, H. Multiple hydrogen bond coordination in three-constituent deep eutectic solvents enhances lignin fractionation from biomass. *Green Chem.* **2018**, *20*, 2711–2721. [[CrossRef](#)]
24. Yang, Q.; Huo, D.; Si, C.; Fang, G.; Liu, Q.; Hou, Q.; Chen, X.; Zhang, F. Improving enzymatic saccharification of eucalyptus with a pretreatment process using MgCl₂. *Ind. Crops Prod.* **2018**, *123*, 401–406. [[CrossRef](#)]
25. Kamireddy, S.R.; Li, J.; Tucker, M.; Degenstein, J.; Ji, Y. Effects and Mechanism of Metal Chloride Salts on Pretreatment and Enzymatic Digestibility of Corn Stover. *Ind. Eng. Chem. Res.* **2013**, *52*, 1775–1782. [[CrossRef](#)]
26. Nemoto, J.; Nakamata, K. All-cellulose material prepared using aqueous zinc chloride solution. *Cellulose* **2021**, *29*, 2795–2803. [[CrossRef](#)]
27. Lin, M.; Shang, X.; Liu, P.; Xie, F.; Chen, X.; Sun, Y.; Wan, J. Zinc chloride aqueous solution as a solvent for starch. *Carbohydr. Polym.* **2016**, *136*, 266–273. [[CrossRef](#)]
28. Wilcox, R.J.; Losey, B.P.; Folmer, J.C.; Martin, J.D.; Zeller, M.; Sommer, R. Crystalline and liquid structure of zinc chloride trihydrate: A unique ionic liquid. *Inorg. Chem.* **2015**, *54*, 1109–1119. [[CrossRef](#)]
29. Liu, W.; Wu, R.; Wang, B.; Hu, Y.; Hou, Q.; Zhang, P.; Wu, R. Comparative study on different pretreatment on enzymatic hydrolysis of corncob residues. *Bioresour. Technol.* **2020**, *295*, 122244. [[CrossRef](#)]
30. Boonchuay, P.; Techapun, C.; Leksawasdi, N.; Seesuriyachan, P.; Hanmoungjai, P.; Watanabe, M.; Takenaka, S.; Chaiyaso, T. An integrated process for xylooligosaccharide and bioethanol production from corncob. *Bioresour. Technol.* **2018**, *256*, 399–407. [[CrossRef](#)]
31. Wen, P.; Liao, H.; Zhu, J.; Xu, Y.; Zhang, J. Production of xylo-oligosaccharides and ethanol from corncob by combined tartaric acid hydrolysis with simultaneous saccharification and fermentation. *Bioresour. Technol.* **2022**, *363*, 127977. [[CrossRef](#)]
32. Luo, Y.; Wei, M.; Jiang, B.; Zhang, M.; Miao, Q.; Fu, H.; Clark, J.H.; Fan, J. A hemicellulose and lignin-first process for corn stover valorization catalyzed by aluminum sulfate in γ -butyrolactone/water co-solvent. *Green Chem.* **2022**, *24*, 7429–7441. [[CrossRef](#)]
33. Ruzene, D.S.; Silva, D.P.; Vicente, A.A.; Goncalves, A.R.; Teixeira, J.A. An alternative application to the Portuguese agro-industrial residue: Wheat straw. *Appl. Biochem. Biotechnol.* **2008**, *147*, 85–96. [[CrossRef](#)]
34. Liao, H.; Li, X.; Lian, Z.; Xu, Y.; Zhang, J. Two-step acetic acid/sodium acetate and xylanase hydrolysis for xylooligosaccharides production from corncob. *Bioresour. Technol.* **2021**, *342*, 125979. [[CrossRef](#)]
35. Liao, H.; Xu, Y.; Zhang, J. Efficient production of xylooligosaccharides and fermentable sugars from corncob by propionic acid and enzymatic hydrolysis. *Bioresour. Technol.* **2021**, *342*, 125680. [[CrossRef](#)]
36. Hao, X.; Xu, F.; Zhang, J. Effect of pretreatments on production of xylooligosaccharides and monosaccharides from corncob by a two-step hydrolysis. *Carbohydr. Polym.* **2022**, *285*, 119217. [[CrossRef](#)]
37. Valladares-Diestra, K.K.; Porto de Souza Vandenberghe, L.; Soccol, C.R. Integrated xylooligosaccharides production from imidazole-treated sugarcane bagasse with application of in house produced enzymes. *Bioresour. Technol.* **2022**, *362*, 127800. [[CrossRef](#)]

38. Bachosz, K.; Zdarta, J.; Nghiem, L.D.; Jesionowski, T. Multienzymatic conversion of monosaccharides from birch biomass after pretreatment. *Environ. Technol. Innov.* **2022**, *28*, 102874. [[CrossRef](#)]
39. Zhang, F.; Lan, W.; Zhang, A.; Liu, C. Green approach to produce xylo-oligosaccharides and glucose by mechanical-hydrothermal pretreatment. *Bioresour. Technol.* **2022**, *344*, 126298. [[CrossRef](#)]
40. Fang, L.; Su, Y.; Wang, P.; Lai, C.; Huang, C.; Ling, Z.; Yong, Q. Co-production of xylooligosaccharides and glucose from birch sawdust by hot water pretreatment and enzymatic hydrolysis. *Bioresour. Technol.* **2022**, *348*, 126795. [[CrossRef](#)]
41. Jiang, Z.; Gao, M.; Ding, W.; Huang, C.; Hu, C.; Shi, B.; Tsang, D.C.W. Selective degradation and oxidation of hemicellulose in corncob to oligosaccharides: From biomass into masking agent for sustainable leather tanning. *J. Hazard. Mater.* **2021**, *413*, 125425. [[CrossRef](#)]
42. Huo Conceptulization, D.; Sun, Y.; Yang, Q.; Zhang, F.; Fang, G.; Zhu, H.; Liu, Y. Selective Degradation of Hemicellulose and Lignin for Improving Enzymolysis Efficiency via Pretreatment Using Deep Eutectic Solvents. *Bioresour. Technol.* **2023**, *376*, 128937. [[CrossRef](#)]
43. Rusanen, A.; Lappalainen, K.; Kärkkäinen, J.; Tuuttila, T.; Mikola, M.; Lassi, U. Selective hemicellulose hydrolysis of Scots pine sawdust. *Biomass Convers. Biorefinery* **2018**, *9*, 283–291. [[CrossRef](#)]
44. Xu, Q.; Chen, L.-F. Ultraviolet spectra and structure of zinc-cellulose complexes in zinc chloride solution. *J. Appl. Polym. Sci.* **1999**, *71*, 1441–1446. [[CrossRef](#)]
45. Zhang, X.F.; Hou, T.; Chen, J.; Feng, Y.; Li, B.; Gu, X.; He, M.; Yao, J. Facilitated Transport of CO₂ through the Transparent and Flexible Cellulose Membrane Promoted by Fixed-Site Carrier. *ACS Appl. Mater. Interfaces* **2018**, *10*, 24930–24936. [[CrossRef](#)]
46. Su, H.; Bi, Z.; Ni, Y.; Yan, L. One-pot Degradation of Cellulose into Carbon Dots and Organic Acids in its Homogeneous Aqueous Solution. *Green Energy Environ.* **2019**, *4*, 391–399. [[CrossRef](#)]
47. Xia, C.; Zhu, S.; Feng, T.; Yang, M.; Yang, B. Evolution and Synthesis of Carbon Dots: From Carbon Dots to Carbonized Polymer Dots. *Adv. Sci.* **2019**, *6*, 1901316. [[CrossRef](#)]
48. Ma, Z.; Wang, J.; Deng, Y.; Wang, Y.; Yan, L. Synthesis of Highly Ion-Conductive Lignin Eutectogels in a Ternary Deep Eutectic Solvent and Nitrogen-Doped 3D Hierarchical Porous Carbons for Supercapacitors. *Biomacromolecules* **2021**, *22*, 4181–4190. [[CrossRef](#)]
49. Bi, Z.; Lai, B.; Zhao, Y.; Yan, L. Fast Disassembly of Lignocellulosic Biomass to Lignin and Sugars by Molten Salt Hydrate at Low Temperature for Overall Biorefinery. *ACS Omega* **2018**, *3*, 2984–2993. [[CrossRef](#)]
50. Fu, H.; Wang, X.; Sang, H.; Hou, Y.; Chen, X.; Feng, X. Dissolution behavior of microcrystalline cellulose in DBU-based deep eutectic solvents: Insights from spectroscopic investigation and quantum chemical calculations. *J. Mol. Liq.* **2020**, *299*, 112140. [[CrossRef](#)]
51. Meenatchi, B.; Renuga, V.; Manikandan, A. Cellulose dissolution and regeneration using various imidazolium based protic ionic liquids. *J. Mol. Liq.* **2017**, *238*, 582–588. [[CrossRef](#)]
52. Yao, L.; Zhou, Z.; Zhang, Z.; Du, X.; Zhang, Q.-L.; Yang, H. Dyeing-Inspired Sustainable and Low-Cost Modified Cellulose-Based TENG for Energy Harvesting and Sensing. *ACS Sustain. Chem. Eng.* **2022**, *10*, 3909–3919. [[CrossRef](#)]
53. Ding, Z.-Y.; Chen, Q.-Y.; Yin, Z.-L.; Liu, K. Predominance diagrams for Zn(II)–NH₃–Cl–H₂O system. *Trans. Nonferrous Met. Soc. China* **2013**, *23*, 832–840. [[CrossRef](#)]
54. Yu, Y.; Cheng, W.; Li, Y.; Wang, T.; Xia, Q.; Liu, Y.; Yu, H. Tailored one-pot lignocellulose fractionation to maximize biorefinery toward versatile xylochemicals and nanomaterials. *Green Chem.* **2022**, *24*, 3257–3268. [[CrossRef](#)]

Disclaimer/Publisher’s Note: The statements, opinions and data contained in all publications are solely those of the individual author(s) and contributor(s) and not of MDPI and/or the editor(s). MDPI and/or the editor(s) disclaim responsibility for any injury to people or property resulting from any ideas, methods, instructions or products referred to in the content.